Int. J. Electrochem. Sci., 11 **(2016)** 3425 - 3435

International Journal of
ELECTROCHEMICAL
SCIENCE
www.electrochemsci.org

MnO_2 Nanosheets-Decorated CuO Nanoneedles Arrays@Cu Foils For Supercapacitors

Xiao Wang[1], *Chen Chen*[2], *Ke Chen*[1,*], *Hao Chen*[1], *Shao Jun Yuan*[2,*]

[1]College of Materials Science and Engineering, Chongqing University, Chongqing 400044, PR China
[2]College of Chemical Engineering, Sichuan University, Chengdu 610065, PR China
[*]E-mail: chenke1_cqu@163.com ; yuanshaojun@gmail.com

Received: 27 January 2016 / *Accepted:* 1 March 2016 / *Published:* 1 April 2016

Using a scaleable chemical method, the ultrathin MnO_2 nanosheets-decorated CuO nanoneedle arrays@Cu sheet has been synthesized and applied as electrodes, while CuO nanoneedles were obtained via an electrochemical deposition at room temperature. Such binder-free Cu/CuO@MnO_2 electrodes were measured by using X-ray diffraction (XRD), and field emission scanning electron microscopy (FESEM) to investigate the structure and morphology. Further electrochemical characterizations revealed that the specific capacitance of samples prepared in 24-hour reaction was as high as 177 mF cm^{-2} at current density 0.5 mA cm^{-2}, with a stable cycling performance of 87.3% retention after 1000 cycles. These findings suggest that the Cu/CuO@MnO_2 electrode is a promising candidate for excellent electrochemical capacitors.

Keywords: copper; copper oxide; manganese dioxide; supercapacitors

1. INTRODUCTION

With the increasingly scare of energy, how reserve energy effectively become an important topic. In recent years, supercapacitors have become a very popular topic due to its excellent storage energy performance such as high specific surface area, short ion diffusion, and electrochemical activity.[1-4]. The principle of supercapacitor to store energy is mainly based on electric double layer capacitors (EDLCs) and pseudocapacitors [5-7]. The pseudocapacitance achieving energy storage depends on rapidly reversible Faradaic reaction in the electrode surface and its nearby, which can produce a lot of capacity, 10 to 100 times that of electric double layer capacitors [8]. MnO_2, one of popular transition metal oxide, is regarded as potential electrode materials for pseudocapacitance due to its low cost, nontoxic, high specific capacitance. It has two different types of operating mechanism

doi: 10.20964/110413

[9-10]. The first is based on adsorption-desorption of the hydrogen ions or cations on the surface of the MnO_2, reaction equation as follows:

$$(MnO_2)_{surface} + M^{n+} + ne^- \longrightarrow (MnO_2^{n-} M^{n+})_{surface} \quad (1)$$

The other mechanism is based on the intercalation/deintercalation of hydrogen ions or cations into MnO_2.

$$MnO_2 + C^+ + e^- \longrightarrow MnOOC \quad (2)$$

The theorial capacitance of MnO_2 can reach to 1370 F g^{-1}, but its relatively low conductivity leads to the poor electrochemical performance in the condition of big volume. In order to obtain superior performance, it not only involves the effective contact between electrolyte and electrode materials, but also rapid transit ions/electrons in the electrode and electrode/electrolyte interface. Therefore, uniting with the active material with large specific surface area, porosity and high conductivity is entailed to MnO_2-based electrodes [11-14].

Copper become ideal composition of electron materials with its low cost, low resistance and good electrical conductivity. However, copper is highly sensitive, impressionable, and hard to control the oxidation [15]. Fortunately, copper oxide is also a good conductor. Copper oxide has received extensive exploration due to its multifunctional and relative abundance in nature, and it has absolute advantages in pseudo-capacitive properties to electrochemical energy storage [16-20]. Surface oxidation treatment cannot only improve the stability of the copper sheet, also be able to keep the electrical conductivity of the material at a relatively high level [15]. In addition, nanostructure of copper oxide provide a large surface area which benefit to improving conductivity.

In addition, the inner porous structures of nanostructured electrodes also allows for more effective electrolyte seepage, and the particle size which reduced dimensions can shorten the length of the electrolyte ion transport and diffusion path, promoting fast kinetics and accelerating charge-discharge rates[21-22].It is extremely common that preparing electrode by nanomaterials in supercapacitor [23].

The structural morphology and particle size play significant roles in determining the physicochemical properties of CuO [24]. According to the related literature, the poor capacitance retention upon cycling is mainly due to the destruction of the crystal structure of CuO during the ion insertion-extraction process [25]. And then, the question is how to modify the composite of copper and copper oxide to achieve maximum efficiency in supercapacitor. With the continuous development of science and technology, electrochemical deposition has rapidly developed into a significant technology to improve performance, and has won a great success. Electrochemical deposition technology is mainly used in the preparation of nanostructure materials, nanocrystalline materials and micro processing technology. The performance of the composite prepared by electrodeposition transcends that prepared by physical methods. What's more, the composition and thickness of sediment can be simply controlled by adjusting the electric current, potential and the concentration of the solution in electrodeposition, and it is always operated at room temperatures [26-29].

Herein, we have prepared composite of MnO_2 nanostructure and Cu/CuO sheets. The Cu sheets with CuO nanoneedle array were fabricated by electrochemical deposition. Clean copper foils were processed by electrochemical deposition in an aqueous KOH solution to obtain CuO nanoneedle array (NNA) films, then the Cu/CuO composite sheets were decorated with MnO_2 nanoflakes followed with

hydrothermal method. The quantities of the MnO_2 nanoflakes deposition can be well controlled by reaction time. The microstructures and electrochemical properties of the three different substances were discussed, which illustrated that the relationship between the quantity of MnO_2 and electrochemical performance.

2. EXPERIMENTAL

2.1 Materials

Copper foils (99.9%, thickness of 0.1 mm) and 1H,1H,2H,2H-Perfluorodecyltriethoxysilane (FAS-17, 97%) were from Xingbo Metal Sample Co. (Tianjin, China) and Sigma-Aldrich Chem Co. (St. Louis, MO), respectively. The raw materials, Potassium permanganate ($KMnO_4$), potassium hydrate (KOH), sodium chloride (NaCl), hydrogen chloride (HCl) and kinds of organic solvents (ethanol, acetone, isopropyl alcohol, tetrahydrofuran) , were of analytical purity and purchased from Alfa Aesar.

2.2 Synthesis of Cu/CuO@MnO_2 nanostructures

The synthesis of the composite can be divided into two parts. In the first step, CuO nanoneedle array deposited on the copper foils were fabricated using electrochemical deposition[15]. Clean copper foils were processed by electrochemical deposition in an aqueous KOH solution to obtain CuO nanoneedle array (NNA) films. After anodization, a faint-blue $Cu(OH)_2$ nanoneedle array film was formed on the copper foils. CuO NNA then came from the transformation by a dehydration reaction. Then, the Cu/CuO composite sheet was decorated with MnO_2 nanoflakes. The MnO_2 nanoflakes were prepared by hydrothermal method. In a typically procedure, Cu/CuO composite sheet was transferred into a 50 ml Teflon-lined stainless steel autoclave and then immersed in 30 mL aqueous solution of $KMnO_4$ (0.03 M). Afterwards, the reactor were maintained at 160 ^oC for different durations (6 h, 24 h). The product was collected, washed with distilled water and dried for several hours. For comparision, bare composite of Cu/CuO was also used to prove the effect of the MnO_2 nanostructrue.

2.3 Characterization

In order to verifying the success of synthesis, chemical composition of the sample was measured by X-ray photoelectron spectroscopy (XRD, D/max 1200, Cu Kα). The structural and morphological investigations of the materials were observed by focused ion beam scanning electron microscopy (ZEISS AURIGA FIB/SEM).

2.4 Electrochemical measurements

The electrochemical measurements were evaluated using a CHI 660E electrochemical workstation with a three-electrode cell system in 1 M KOH electrolyte. The cyclic voltammetry was

detected under the voltage window between -0.2 V and 0.6 V, which is used to determine the capacitive behaviors of these composites. The galvanostatic charge-discharge curves were taken to reflect the properties about the stability. The electrochemical impedance spectroscopy (EIS) was used to measure the electrochemical behaviors of the different electrodes, which were carried out with the frequency between 10 kHz and 0.01 Hz.

3. RESULTS AND DISCUSSION

3.1 Structure and morphology

The structure of the materials fabricated with different reaction times were measured by XRD (Fig. 1). Diffraction peaks are composed of three phases, Cu, CuO and MnO_2. The diffraction peaks could be attributed to the (001) and (002) planes of MnO_2, and the other diffraction could be assigned to (11-1), (111), (11-2) and (11-3) planes of CuO. The dominant peaks clearly indicated the successful synthesis, and no characteristic peaks of impurities were detected.

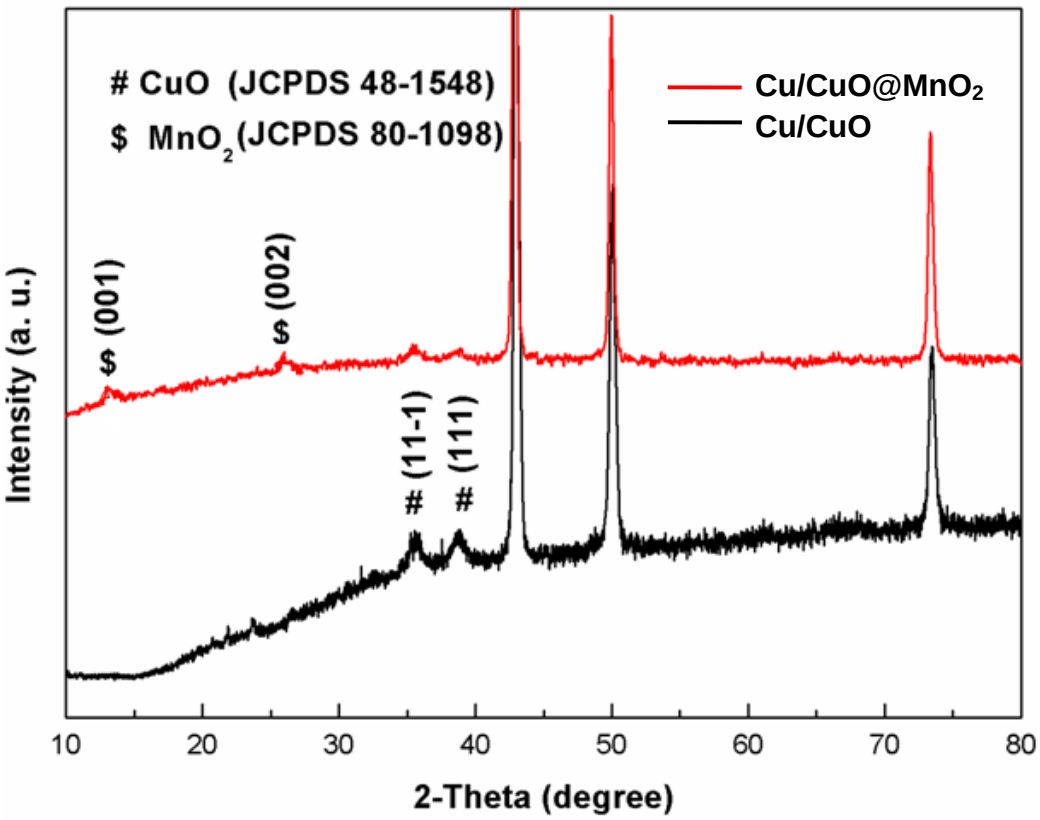

Figure 1. XRD patterns of the Cu/CuO @MnO_2 .

The chemical routes to fabricate the composite of Cu/CuO@MnO_2 can be illustrated in Fig. 2. The experiment can be accomplished by two steps. The copper foil was cleaned with water and kinds of solutions, and stored in the vacuum desiccators.

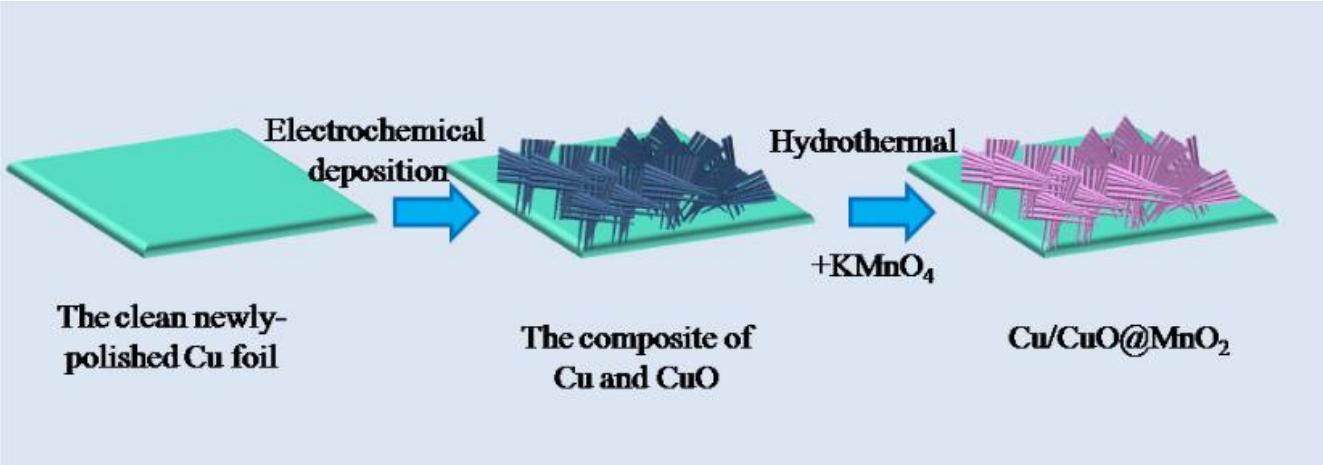

Figure 2. Schematic illustration showing the synthetic procedure of the MnO_2 nanostructure arrays directly on Cu/CuO sheet.

At the initial process, CuO nanoneedle array was obtained by electrochemical deposition from Cu foil in an aqueous KOH solution. The chemical reactions as follows [15]:

$$Cu(s) \longrightarrow Cu^{2+} + 2e^- \quad (3)$$

$$Cu^{2+} + 2OH^-(aq) \longrightarrow Cu(OH)_2(s) \quad (4)$$

$$Cu(OH)_2(s) \longrightarrow CuO(s) + H_2O \quad (5)$$

And then, we choose the strong oxidant aqueous $KMnO_4$ solution as the raw material to prepare MnO_2. MnO_2 nanosheets were obtained by hydrothermal and coating on the Cu foil which was decorated with CuO nanoneedle array. The quantity of the MnO_2 nanosheets can be controlled by adjusting the reaction time.

The SEM images of products with different reaction times were shown in Fig. 3. Firstly, we can see the Cu foil was covered with CuO nanoneedle arrays equably (Fig. 3a). The CuO nanoneedle arrays are very thin (Fig. 3b), and one bunch contains dozens of nanowires with the diameter of ~1-2 μm. As show in Fig. 3c and d, nanosheets on the nanoneedle arrays were clearly seen from the SEM images, and such nanosheets are well distributed on the surface of the nanoneedles. The result indicated that the synthesis of MnO_2 nanosheets with Cu/CuO for 6 h is satisfactory. The morphologies of the composite for 24 h are presented in Fig. 3e and f. Compared with the reaction time for 6 h, the result of the product for 24 h shows a large increase in the number of MnO_2 nanosheets. It is obvious that the thickness of the nanoneedle arrays increased due to the combination of MnO_2 and Cu/CuO composite.

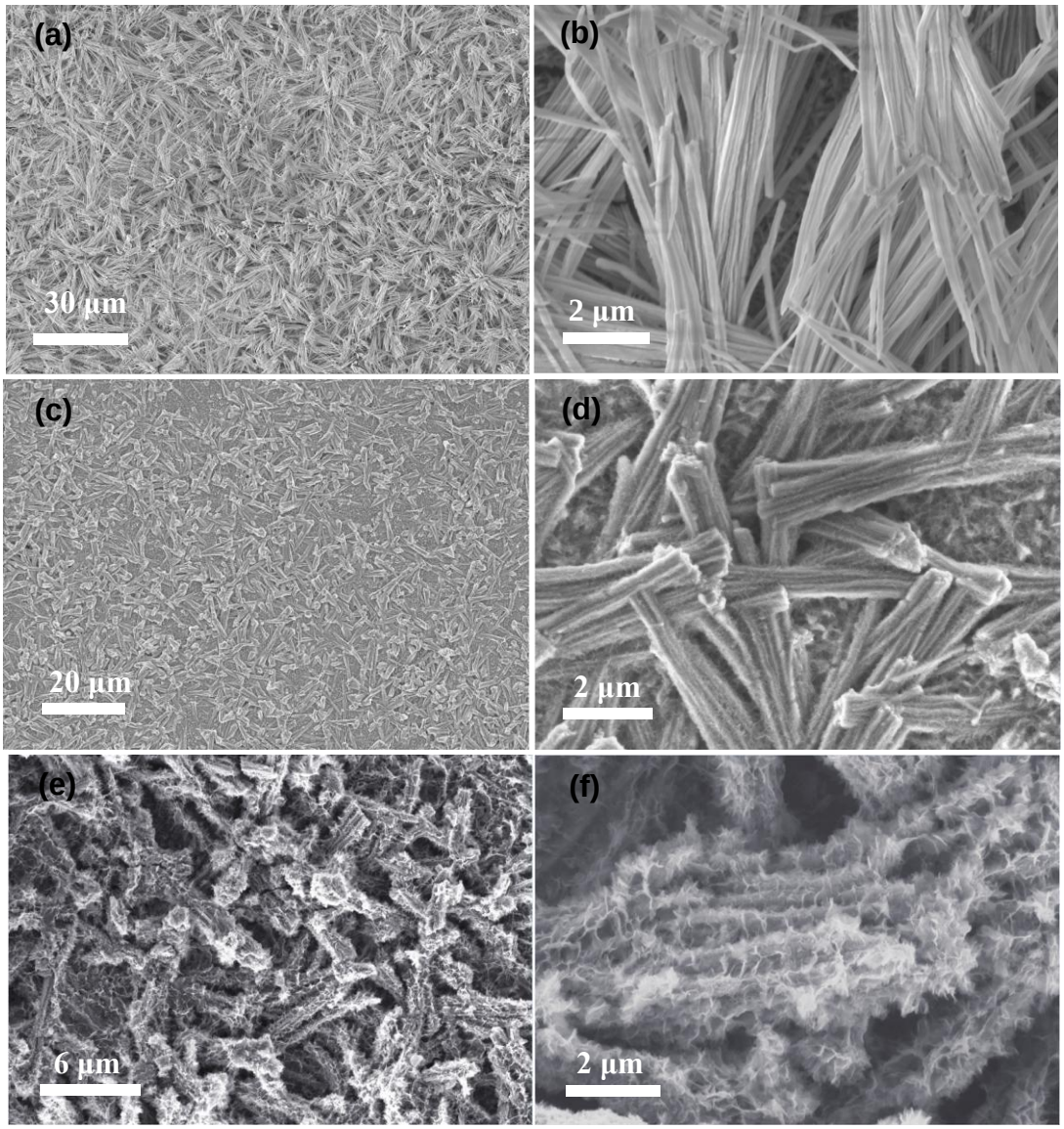

Figure 3. SEM images of Cu/CuO@MnO_2 obtained at different reaction times: (a-b) 0 h, (c-d) 6 h, (e-f) 24 h.

3.2 Electrochemical properties of the Cu/CuO@MnO_2 nanostructures

For better understanding of the electrochemical properties of the as-prepared nanocomposites, the samples need to be made into supercapacitor electrodes for detections. Electrochemical tests were characterized using a three-electrode configuration, and carried out with cyclic voltammetry, galvanostatic charge/discharge and impedance measurements. Cyclic voltammograms of Cu/CuO@MnO_2 nanostructures in the potential range -0.2-0.6 V vs. SCE are shown in Fig. 4a at the scan rate of 100 mV s^{-1} in a 1 M KOH aqueous electrolyte. The CV curves of Cu/CuO electrode exhibit an irregular shape. The CV curves for the two samples decorated with MnO_2 nanosheets were very similar and quite different from the CV curve of Cu/CuO electrode, which indicated that 2D MnO_2 nanosheets increase the external surface to change the capacitance. In addition, the large

increment of the CV integrated area suggests that the mass of MnO_2 impacted the capacitance of the composite, the larger quantities of MnO_2, the larger capacitance of the composite. Furthermore, the CV curves of Cu/CuO@MnO_2 have no obvious redox-peak position, exhibiting stable electrochemical property， and the symmetrical shapes prove high reversibility of the electrodes. The Cu/CuO electrode was not discussed in the following due to its barren electrochemical properties.

Galvanostatic charge-discharge curves of Cu/CuO@MnO_2 electrodes were evaluated with an electrochemical window of -0.2-0.5 V at current densities of 10 mA cm^{-2} are shown in Fig. 4b. For linear charge images, discharge curve roughly mirror symmetry to the charge curve. With continuous discharging, slope of the discharge curve slightly decreased. We can see from the graph that the product for 24 h looks better than 6 h in electrochemical performance, and the discharge time of the former is about 2 times longer than the latter. The specific capacitances are measured according to the following equation:

$$C_s=It/\Delta Vs \qquad (6)$$

where C_s is specific capacitance (mF cm^{-2}), I is the charge-discharge current (mA), t is discharge time and ΔV means the range of voltage window which from -0.2 to 0.6 V, s is the area of electrode (cm^{-2}).

As calculated from Galvanostatic charge-discharge curves, the specific capacitances were shown in Fig. 4c. By comparison, the sample for 24 h yielded higher specific capacitance under the condition of constant current density. More specifically, the specific capacitance of 24 h was as high as 177 mF cm^{-2} at current density 0.5 mA cm^{-2}, which higher than 72 mF cm^{-2} for 6 h. The superior power capability of the Cu/CuO@MnO_2 electrode for 24 h could be attributed to its fast electrode kinetics. Fig.4d compares the electrochemical impedance spectroscopy (EIS) spectra of Cu/CuO@MnO_2 electrodes for different reaction time. EIS is used to test ion transfer and electrical conductivity at open circuit potential in the supercapacitor.

In this equivalent circuit from Fig. 4d, R_s, R_{ct}, CPE, and Z_w refer to internal resistance, charge-transfer resistance, capacitance of the double layer, and Warburg impedance, respectively [30]. Internal resistance (R_s) has a total of the intrinsic resistance of active materials, the contact resistance at the active material/current collector interface and the ionic resistance of electrolyte. The interfacial charge transfer resistance (R_{ct}) can be roughly estimated by the diameters of semicircles in the figure of EIS [31]. It is obviously that the electrode for 24 h showed a much smaller charge transfer resistance compared to that of the electrode for 6 h. The smaller charge transfer resistance of the electrode for 24 h is attributed to the closer contact CuO with the MnO_2, which is consistent with the specific capacitance of these electrodes. Therefore, the quantity of MnO_2 was taken into account to increase electrical conductivity, to increase the surface area, and to decrease the charge-transfer resistance.

Based on the above analysis, we know that the Cu/CuO@MnO_2 electrode for 24 h have a much higher capacitance than the electrode for 6 h at the same scan rate. To calculate the potential applications in electrochemical capacitors, CV curves of the Cu/CuO@MnO_2 electrode for 24 h and the corresponding Galvanostatic charge-discharge curves are shown in Fig. 5a and b respectively. The CV curves of the Cu/CuO@MnO_2 electrodes are very similar and display the distorted rectangularity shapes in Fig. 5a under these conditions of the scan rate range 10-100 mV s^{-1} and potential range -0.2-

0.6 V vs. SCE. The irregular curves indicated that the capacitive behaviors of Cu/CuO@MnO_2 electrode primarily stem from Faradic redox reactions.

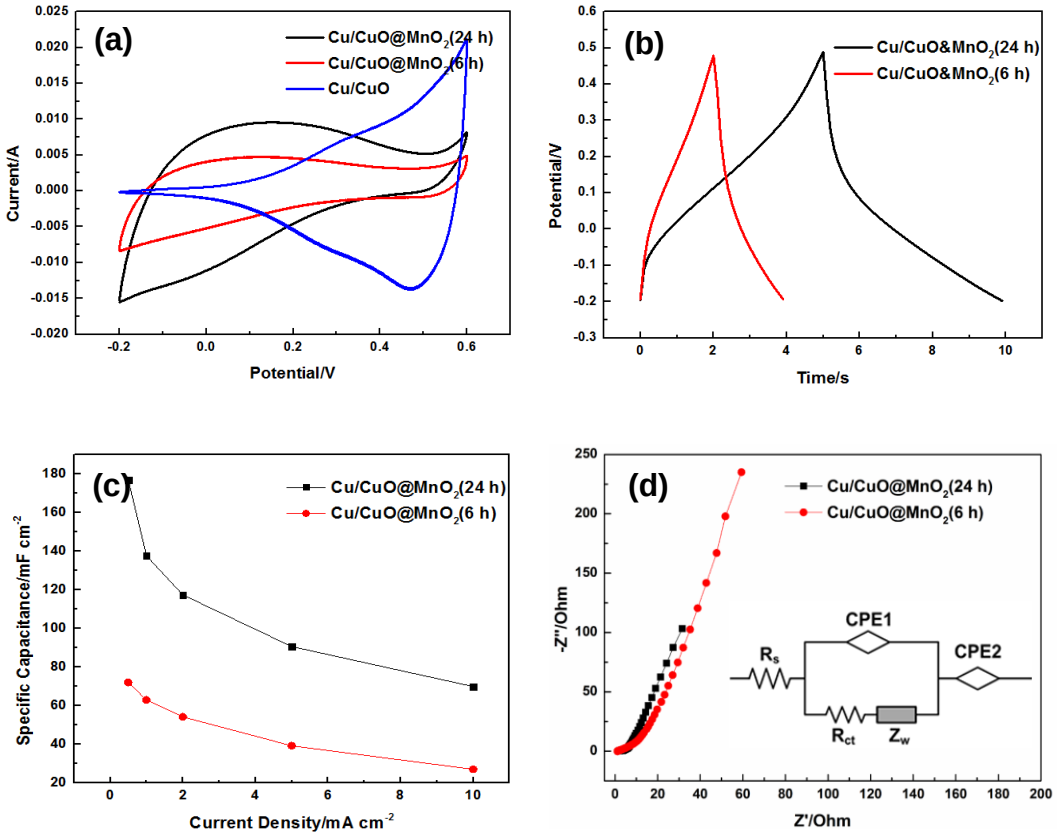

Figure 4. (a) Cyclic voltammograms of Cu/CuO@MnO_2 nanostructures with different times at the scan rate of 100 mV s^{-1} in a 1 M KOH aqueous electrolyte, (b) Galvanostatic charge-discharge curves of Cu/CuO@MnO_2 electrodes at current densities of 10 mA cm^{-2};(c) Specific capacitance of the products for 6 h and 24 h under different current densities;(d) Nyquist plots of the electrodes before the cycles.

Herein, the CV scans was the result of the synergistic effect between MnO_2 and CuO pseudocapacitance behavior. And the pseudocapacitance behavior of CuO was associated with the following reaction [17,24]:

$$Cu_2O + 2OH^- \longrightarrow 2CuO + H_2O + 2e^- \quad (6)$$

$$Cu_2O + H_2O + 2OH^- \longrightarrow 2Cu(OH)_2 + 2e^- \quad (7)$$

$$CuOH + OH^- \longrightarrow CuO + H_2O + e^- \quad (8)$$

$$CuOH + OH^- \longrightarrow Cu(OH)_2 + e^- \quad (9)$$

Galvanostatic charge-discharge curves were performed with electrochemical window of -0.2-0.5 V. Similar charge-discharge curves were observed for all the current densities. Good symmetry and fairly linear slopes were observed in the charge-discharge curves of the Cu/CuO@MnO_2 electrode, indicating a superior electrochemical capacitive characteristic.

The specific capacitance obtained from the discharge curves was calculated to be 177 mF cm^{-2} at a low current density of 0.5 mA cm^{-2}. As the current density increased to 10 mA cm^{-2}, the specific capacitance can still reach 39.55% of capacitance was retained. The good rate capability is attributed to

the good conductivity of the electrode and small charge transfer resistance. The long-term cyclic stability of SCs is another critical issue in practical use. Fig. 5c shows the cycling performance of Cu/CuO@MnO_2 electrode at the current density of 5 mA cm^{-2}. With the first cycle capacitance (90 mF cm^{-2}), the Cu/CuO@MnO_2 electrode delivers a capacitance of 78.57 mF cm^{-2} during the 1000th cycle. The capacitive retention is 87.3% after 1000 cycles and about 99.9% per cycle, indicating favourable cyclability. The SEM images of the Cu/CuO@MnO_2 electrode for 24 h after 1000 cycles demonstrated that the structure was maintained rather well.

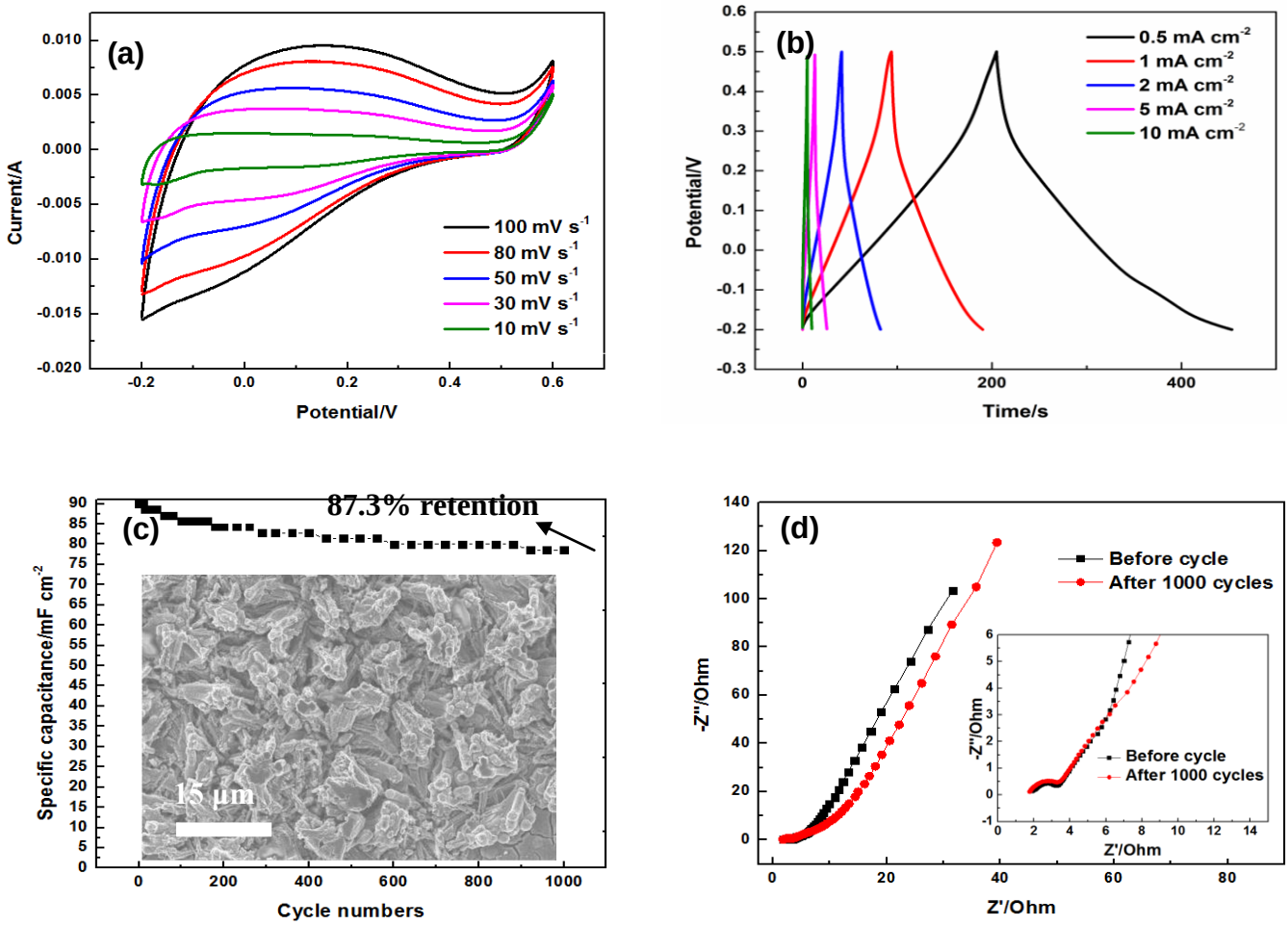

Figure 5. (a) Cyclic voltammograms of Cu/CuO@MnO_2 nanostructures for 24 h at different scan rate (10, 30, 50, 80 and 100 mV s^{-1}) in a 1 M KOH aqueous electrolyte; (b) Corresponding charge-discharge curves of Cu/CuO@MnO_2 electrodes at different current densities (0.5, 1, 2, 5 and 10 mA cm^{-2}); (c) Cycling performance at the current density of 5 mA cm^{-2}(the inset shows SEM image of Cu/CuO @MnO_2 after 1000 cycles) ; (d) Electrochemical impedance spectrum of the electrodes in the frequency range from 0.01 Hz to 10 kHz (the inset is the magnified plot).

Nyquist plots were measured before and after 1000 cycles to further investigate the cycling stability, as shown in Fig. 5d (the inset is the magnified plot). The main distinction is the slope of the straight line in low frequency. The impedance of the electrode before cycle increase sharply indicating low diffusive resistance for intercalation/deintercalation of cations. In comparison, the electrode shows larger diffusive resistance after 1000 cycles because the channels for intercalation/deintercalation were hindered in the cycles. However, almost no different between the two semicircle diameters in high and

middle frequency indicated that the charge transfer resistance is constant. This result corresponds to the stable structure of the material in the reaction.

4. CONCLUSIONS

We have developed a facile strategy for the growth of MnO_2 nanostructrue on the Cu/CuO sheet. Investigation of the quality of MnO_2 which controlled by reaction times indicated that MnO_2 played an important role in providing the excellent capacitance and decreasing resistance. Compared with other composite MnO_2@Cu/CuO (reaction time are 0 h and 6 h respectively), the formation of MnO_2@Cu/CuO for 24 h offers remarkably enhanced specific capacitance and stability, with a lower resistance and higher cycle performance. The specific capacitance of Cu/CuO@MnO_2 for 24 h reached at 177 mF cm^{-2} in the current density 0.5 mA cm^{-2}, which was higher than 72 mF cm^{-2} for 6 h. The capacitive retention of Cu/CuO@MnO_2 for 24 h is 87.3% after 1000 cycles and about 99.9% per cycle, indicating favorable cyclability. In principle, considering the low cost and stable properties in electrochemistry, Cu/CuO@MnO_2 nanostructures have the potential applications in supercapacitors.

ACKNOWLEDGEMENT
The authors gratefully acknowledge the financial supports provided by State Education Ministry and Fundamental Research Funds for the Central Universities (Chongqing University).

References

1. X. H. Lu, M. H. Yu, G. M. Wang, Y. X. Tong, Y. Li, *Energy Environ. Sci.*, 7 (2014)2160.
2. G.P. Wang, L. Zhang, J. J. Zhang, *Chem. Soc. Rev.*, 41 (2012)797.
3. M. Q. Xue, F. W. Li, J. Zhu, H. Song, M. N. Zhang, T. B. Cao, *Adv. Funct. Mater.*, 22 (2012) 1284
4. H. L. Wang, Chris M. B. Holt, Z. Li, X. H. Tan, Babak Shalchi Amirkhiz, Z.W. Xu, Brian C. Olsen, Tyler Stephenson, David Mitlin, *Nano Res.*, 5(9): (2012)605.
5. K. W. Qiu , Y. Lua , D. Y. Zhang, J. B. Cheng, H. L. Yan, J. Y. Xu, X. M. Liu, J. K. Kim, Y. S. Luo, *Nano Energy*, 11 (2015)687.
6. R. B. Rakhi, Wei Chen, Dongkyu Cha, and H. N. Alshareef , *Nano Lett.*, 12 (2012) 2559.
7. K. F. Chen, S. Yin, D. F. Xue, *Nanoscale*, 7 (2015) 1161.
8. H. Xia, C. Y. Hong, X. Q. Shi, B. Li, G. L. Yuan, Q. F. Yao, J. P. Xie, *J. Mater. Chem. A*, 3(2015) 1216.
9. Y. Munaiah, B. G. S. Raj, T. P. Kumar, P. Ragupathy, *J. Mater. Chem. A*, 1 (2013) 4300.
10. S. H. Li, L. Qi, L. H. Lu, H. Y. Wang, *RSC Advances*, 2 (2012) 3298.
11. G. X. Wang, H. F. Xu, L. Lu, H. Zhao, *J. Mater. Chem. A*, 3 (2015) 1127.
12. M. Yu , J. P. Chen, J. H. Liu, S. M. Li, Y. X. Ma, J. D. Zhang, J. W. An, *Electrochimica Acta* 151 (2015) 99.
13. H. W. Chang, Y.R Lu, J. L. Chen, C.L. Chen, J. F. Lee, J. M. Chen, Y. C. Tsai, C. M. Chang, P. H. Yeh, *Nanoscale*, 7 (2015) 1725.
14. M. Kuang, X. Y. Liu, F. Dong, Y. X. Zhang, *J. Mater. Chem. A*, 3 (2015) 21528
15. F. Xiao, S. J. Yuan, B. Liang, G. Q. Li, S. O. Pehkonenc, T. J. Zhang, *J. Mater. Chem. A*, 3(2015) 4374.
16. S. E. Moosavifard, M. F. El-Kady, M. S. Rahmanifar, R. B. Kaner, M. F. Mousavi, *ACS Appl. Mater. Interfaces*, 7 (2015) 4851.

17. J. F. Huang, H. L. Li, Y. H. Zhu, Q. L. Cheng, X. L. Yang, C. Z. Li, *J. Mater. Chem. A*, 3(2015) 8734.
18. M. Kuang, T. T. Li, H. Chen, S. M. Zhang, L. L. Zhang, Y. X. Zhang, *Nanotechnology*, 26 (2015) 304002.
19. Y. X. Zhang, M. Huang, M. Kuang, C. P. Liu, J. L. Tan, M. Dong, Y. Yuan, X. L. Zhao, Z. Q. Wen , *Int. J. Electrochem. Sci.*, 8 (2013) 1366.
20. G.J. Navathe, D.S. Patil, P.R. Jadhav, D.V. Awale, A.M. Teli, S.C. Bhise, S.S. Kolekar,M.M. Karanjkar, J.H. Kim, P.S. Pati, *Journal of Electroanalytical Chemistry*, 738 (2015) 170.
21. S. Chen, W. Xing, J. J. Duan, X. J. Hu,S. Z. Qiao, *J. Mater. Chem. A*, 1 (2013) 2941.
22. Q. F. Zhang, G. Z. Cao, *Nano Today*, 6 (2011) 91.
23. G. D. Moon, S. Ko, Y. Min, J. Zeng, Y. Xia, U. Jeong, *Nano Today*, 6 (2011) 186.
24. G. H. Qiu, S. Dharmarathna, Y. S. Zhang, N. Opembe, H. Huang, S. L. Suib, *J. Phys. Chem. C*, 116 (2012) 468.
25. Z. Q. Zhang, C. C. Ma, M. Huang, F. Li, S. J. Zhu, C. Hua, L. Yu, H. L. Zheng, X. B. Hu, Y. X. Zhang, *J Mater Sci: Mater Electron*, 26 (2015) 4212.
26. O. Lupan, T. Pauporte, L. Chow, B. Viana, F. Pelle, L.K. Ono, B. Roldan Cuenya, H. Heinrich, *Applied Surface Science*, 256 (2010) 1895.
27. J. Elias, C. Le´vy-Cle´ment, M. Bechelany, J. Michler, G. Y. S. Wang, Z. Wang, L. Philippe, *Adv. Mate* , 22 (2010) 1607.
28. J. H. Bang, P.V. Kamat, *Adv. Funct. Mater.*, 20 (2010) 1970.
29. X. N. Wang, H. J. Zhu, Y. M. Xu, H. Wang, Y. Tao, S. K. Hark, X. D. Xiao, Q. Li, *ACS.NANO*, 6 (2010) 3302.
30. S. H. Aboutalebi, A. T. Chidembo, M. Salari, K. Konstantinov, D. Wexler, H. K. Liu, S. X. Dou, *Energy Environ. Sci.*, 4 (2011)1855.
31. Y. Lei, J. Li, Y. Y. Wang, L. Gu, Y. F. Chang, H. Y. Yuan, D. Xiao, *ACS Appl. Mater. Interfaces*, 6 (2014) 1773.